

LOCAL ORDER OF THE TRANSITION METALS FOR THE SUBSTITUTION $(Co_{1-y}Cu_y)_2Al(OH)_6Cl \cdot nH_2O$ ($0 \leq y \leq 1$) IN A COPPER-ALUMINUM-LAYERED DOUBLE HYDROXIDE-LIKE PHASE

FABRICE LEROUX^{1,*}, EL MOSTAFA MOUJAHID¹, HERVÉ ROUSSEL², ANNE-MARIE FLANK², VALÉRIE BRIOIS²
AND JEAN-PIERRE BESSE¹

¹ Laboratoire des Matériaux Inorganiques, CNRS-UPRES-A n°6002, Université Blaise Pascal, 63177 Aubière cédex, France

² LURE, Centre Universitaire Paris Sud, Bât 209D, BP 34, 91898 Orsay cédex, France

Abstract—The substitution in layered double hydroxide-like phases (LDH) of composition $(Co_{1-y}Cu_y)_2Al^{3+}(OH)_6Cl \cdot nH_2O$ ($0 \leq y \leq 1$) was studied by X-ray diffraction and X-ray absorption spectroscopy. It was found that the lamellar character is maintained over the entire range of the substitution. The local order for the composition {Co₂Al} is typical of brucite-like sheets, whereas segregation into small domains may explain the results obtained when the percentage of Cu atoms is increased. The {Cu₂Al} end-member material presents a local order around the Cu atoms closely related to the botallackite structure as present in basic layered Cu salts, with the presence of two distinct Cu–Cu distances.

Key Words—Botallackite Structure, Layered Double Hydroxide, X-ray Absorption Spectroscopy.

INTRODUCTION

Hydrotalcite-like layered double hydroxides (LDH) can be described as positively charged brucite sheets in which some of the Mg²⁺ ions have been substituted by trivalent ions such as Al³⁺, Cr³⁺, etc. The excess positive charge is counterbalanced by anions present in the interlayer space. In the following, LDH materials are noted as {M_x^{II}M^{III}A} with x being the ratio between the divalent and trivalent cations and A the interlayered anion. The synthetic anionic clays were prepared by the ‘chimie douce’ method. The question of homogeneity in the layers was questioned for some LDHs and other clay materials (Vucelic *et al.*, 1997; Manceau and Calas, 1986; Roussel *et al.*, 2000). This is of importance for catalytic applications for which large surface area combined with good metal dispersion is needed. Interstratification was observed, depending on the chemical composition in the LDH system {Co_xAl-CO₃²⁻} (Thompson *et al.*, 1999). Organization may also be present, e.g. superlattices are observed in pyroaurite {Mg_{2.3}Fe-CO₃²⁻} (Vucelic *et al.*, 1997) and in {LiAl₂-OH} (Thiel *et al.*, 1993) (Besserguenev *et al.*, 1997). For the latter, the ordering of the cations is explained with the Li ions migrating into the empty octahedral sites available in the gibbsite virgin framework. For other systems, the lack of this ordering may be caused by the large difference in radius between the M^{II} and M^{III} cations (Bellotto *et al.*, 1996). This is the case for numerous LDH materials presenting Al³⁺ as trivalent

cations. The interlayered anions may also induce an organization as shown by the highly ordered two-dimensional superlattice present in the {Zn₂Al-SO₄²⁻} LDH sample (Bookin *et al.*, 1993).

In the present paper, the local structure of {Cu₂Al} is studied. The reasons for our interest include the possibility of heterogeneous catalysis combined with oxidation-reduction reaction (Trombetta *et al.*, 1997; Shimizu *et al.*, 2000). The {Cu₂Al} sample is present as a disordered material, making it difficult to establish its structural affiliation to the LDH class of materials. It was shown that the {Cu₂Al} material, after sintering, presents a well-dispersed mixture of CuO and CuAl₂O₄ phases (Alejandre *et al.*, 1999).

Starting with a well-crystallized {Co₂Al} LDH phase, the substitution between Co²⁺ and Cu²⁺ cations for the LDH material {(Co_{1-y}Cu_y)₂Al-Cl} was studied by X-ray diffraction (XRD) and X-ray absorption spectroscopy (XAS) at Co and Cu *k*-edge. It is noteworthy that the two divalent cations have the same ionic radius. The XAS technique is known to be suitable for the study of local order. Moreover, this highly selective technique provides information on substitution (Aitchison *et al.*, 1999) and in situations where a slight change of the local environment occurs (Carrado and Wasserman, 1996; Leroux *et al.*, 2001a,b). As backscatterers, the two cations are indistinguishable. Comparison of the spectra recorded at both *k*-edges provides some information on the local environment surrounding each cation. The main purpose of this work is to understand whether {Cu₂Al-Cl} is retaining a LDH-type structure, and how cations are accommodating the strongly destabilizing Jahn-Teller effect of the Cu²⁺ ions to sustain the octahedra edge-sharing LDH sheets.

* E-mail address of corresponding author:
leroux@chimtp.univ-bpclermont.fr

MATERIALS AND METHODS

Synthesis

$(\text{Cu}_y\text{Co}_{1-y})_2\text{Al}$ hydrotalcite-like materials were prepared by the co-precipitation method according to Miyata (1983). A 250 ml solution containing Al, Cu and Co of total cation concentration ($\text{Co}+\text{Cu}+\text{Al}$) of 10^{-2} M was prepared from $\text{AlCl}_3 \cdot 6\text{H}_2\text{O}$ (Aldrich), $\text{CoCl}_2 \cdot 6\text{H}_2\text{O}$ (Aldrich) and $\text{CuCl}_2 \cdot 6\text{H}_2\text{O}$ (Aldrich). The solution is added dropwise to decarbonated water. The pH is kept constant at 10.7. The preparation is performed under N_2 gas flowing to avoid any contact with atmospheric CO_2 . The slurry is aged overnight, centrifuged, and then washed several times with decarbonated water and finally dried at room temperature.

Analysis

The results of elemental analyses performed at the Centre d'Analyse de Vernaison, France, are reported in Table 1. Results concerning Co:Cu:Al (y and M^{II} to M^{III} ratio) follow the initial salt concentration.

Powder X-ray diffraction (PXRD) profiles were obtained using a Siemens D500 X-ray diffractometer with a diffracted beam monochromator $\text{CuK}\alpha$ source. The Fourier transform infrared (FTIR) spectra were recorded on a Perkin-Elmer 2000 FT spectrometer employing the KBr dilution technique.

X-ray absorption spectroscopy

Co and Cu k -edge XAS study was performed at LURE (Orsay, France) using X-ray synchrotron radiation emitted by the DCI storage ring (1.85 GeV positrons, average intensity of 250 mA) at the D44 beam line. The data were collected at room temperature in transmission mode at Co and Cu k -edges (7,708.9 and 8,978.9 eV, respectively). A double-crystal Si (111) monochromator scanned the energy in 2 eV-steps from 100 eV to 900 eV for each k -edge, and three spectra were recorded for each sample. An accumulation time of 2 s was used per point. In the near-edge (XANES) regions, two spectra were recorded from 7,670 to 7,810 eV for the Co k -edge and from 8,950 to 9,100 eV for the Cu k -edge with a 0.25 eV and 1 s of

accumulation time per point, using a Si (311) monochromator. Extraction and analysis of EXAFS data was performed following standard procedures as reported elsewhere (Leroux *et al.*, 1999; Malherbe *et al.*, 1999). The $\chi(k)$ signal was fitted by using the classic plane-wave single scattering approximation:

$$\chi(k) = S_0^2 \sum A_i(k) \sin[2k.r_i + \phi_i(k)],$$

with $A_i(k)$ amplitude equal to $(N_i/k.r_i^2)F_i(k)\exp(-2k^2\sigma_i^2)$

where r_i is the interatomic distance, ϕ_i the total phase shift of the i^{th} shell, N_i the effective coordination number, σ_i the Debye-Waller factor and $F_i(k)$ the backscattering amplitude. The residual ρ factor is defined as $\rho = [\Sigma(k^3\chi_{\text{exp}}(k) - k^3\chi_{\text{theo}}(k))^2/\Sigma(k^3\chi_{\text{exp}}(k))^2]^{1/2}$. The commonly accepted fitting accuracy is of 0.02 Å for the distance and $\approx 20\%$ for the number of neighbors.

RESULTS

XRD pattern

The PXRD diffraction patterns of $(\text{Co}_{1-y}\text{Cu}_y)_2\text{Al}(\text{OH})_6\text{Cl}_n\text{H}_2\text{O}$ ($0 \leq y \leq 1$) are typical of layered material with a series of basal reflections (Figure 1). The pattern of the $\{\text{Co}_2\text{Al}-\text{Cl}\}$ material exhibits sharp diffraction peaks, characteristic of the layered double hydroxide structure. The $\{\text{Co}_2\text{Al}-\text{Cl}\}$ pattern was refined using the $R\bar{3}m$ space group in rhombohedral symmetry (eight distinct d_{hkl} distances were indexed). The cell parameters a and c (equal to three times the interlamellar distance) are equal to 3.064 and 23.27 Å, respectively. For the substituted materials, the 110 and 113 diffraction peaks are overlapped, making any refinements ambiguous. The 110 peak is usually used for the calculation of the parameter a . For $y \geq 0.9$, the XRD peaks are broad, suggesting that the phases are highly disordered. Nevertheless crystallized by-products such as malachite, gibbsite, gerhardite or paratacamite are not observed. The coherence length along the stacking direction was estimated from the 006 fwhm using the Scherrer formula: $D_{hkl} = K\lambda/\beta_{1/2}\cos\theta$, where λ is the X-ray wavelength, θ the diffraction angle, $\beta_{1/2}$ the width at half maximum intensity and K a

Table 1. Chemical compositions as a function of y in $(\text{Co}_{1-y}\text{Cu}_y)_2\text{Al}(\text{OH})_6\text{Cl}_n\text{H}_2\text{O}$ ($0 \leq y \leq 1$) based on elemental analysis.

Samples (y)	y_{meas}	$M^{\text{II}}/M^{\text{III}}_{\text{meas}}$	Formulae
0	0	2.18	$\text{Co}_{0.68}\text{Al}_{0.31}(\text{OH})_2\text{Cl}_{0.30}(\text{CO}_3^{2-})_{0.02} \cdot 0.62\text{H}_2\text{O}$
0.1	0.09	2.12	$\text{Cu}_{0.06}\text{Co}_{0.62}\text{Al}_{0.32}(\text{OH})_2\text{Cl}_{0.30}(\text{CO}_3^{2-})_{0.02} \cdot 0.58\text{H}_2\text{O}$
0.25	0.025	2.06	$\text{Cu}_{0.17}\text{Co}_{0.49}\text{Al}_{0.32}(\text{OH})_2\text{Cl}_{0.31}(\text{CO}_3^{2-})_{0.02} \cdot 0.81\text{H}_2\text{O}$
0.50	0.50	2.00	$\text{Cu}_{0.31}\text{Co}_{0.31}\text{Al}_{0.31}(\text{OH})_2\text{Cl}_{0.30}(\text{CO}_3^{2-})_{0.02} \cdot 0.75\text{H}_2\text{O}$
0.75	0.75	2.01	$\text{Cu}_{0.50}\text{Co}_{0.16}\text{Al}_{0.33}(\text{OH})_2\text{Cl}_{0.32}(\text{CO}_3^{2-})_{0.01} \cdot 0.50\text{H}_2\text{O}$
0.90	0.90	2.19	$\text{Cu}_{0.60}\text{Co}_{0.08}\text{Al}_{0.31}(\text{OH})_2\text{Cl}_{0.31}(\text{CO}_3^{2-})_{0.01} \cdot 0.63\text{H}_2\text{O}$
1	1	2.30	$\text{Cu}_{0.69}\text{Al}_{0.30}(\text{OH})_2\text{Cl}_{0.30}(\text{CO}_3^{2-})_{0.01} \cdot 0.90\text{H}_2\text{O}$

meas: measured

constant usually taken as 0.9. A domain of 460 Å was found for the $\{\text{Co}_2\text{Al}\}$ material, smaller than the Cu substitution of 150 Å for $\{\text{Cu}_2\text{Al}\}$. This corresponds to ~60 and 20 stacked layers, respectively. This also shows that Cu cations induce a strong distortion in the interlamellar organization and for the stacking sequence. No trace of $\text{Cu}(\text{OH})_2$ was found for the Cu-rich phases. Some broad shoulders are observed at ~17, 30 and $40^\circ 2\theta$, and this may be the manifestation of an amorphous phase, probably $\text{Cu}_2(\text{OH})_3\text{Cl}$ paratacamite (Figure 3).

At the first glance, synthetic clay materials retain a hydrotalcite-like structure while increasing intralayer disorder with the Cu substitution. With a percentage of trivalent cations constant with the substitution, *i.e.* nominal layer charge also constant, the interlamellar distance should remain the same. A slight variation of the basal spacing is observed (Figure 2). The shrinking of the interlayer space is due to the increase of electrostatic attraction between the positive LDH layers and the negatively charged anions. In the absence of such a modification, the variation has to be explained by a corrugation of the sheets, as observed for $\{\text{Cu}_2\text{Cr}-\text{Cl}\}$ LDH material (Roussel *et al.*, 2000). The particular

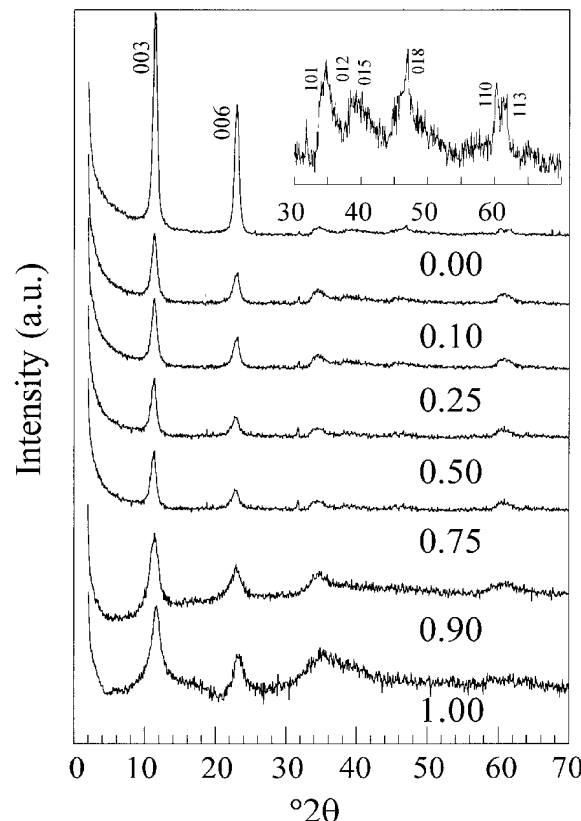


Figure 1. XRD patterns of $(\text{Co}_{1-y}\text{Cu}_y)_2\text{Al}(\text{OH})_6\text{Cl}\cdot n\text{H}_2\text{O}$ ($0 \leq y \leq 1$) LDH-like materials. The values for y are reported. The 30 to 70° region is magnified for $\{\text{Co}_2\text{Al}\}$ composition in the inset. The reflections are identified.

atomic arrangement then induces an increase in the thickness of the brucite-like sheet (Velu *et al.*, 1998).

In order to improve the crystallinity, hydrothermal treatment was carried out; the samples were placed in a sealed Teflon® tube, and kept at 120°C for two days under autogenous pressure. An increase in the crystallinity is observed with the heat treatment for the materials containing less than half of the Cu cations as M^{II} (Figure 3). For greater Cu^{2+} contents, the layered structure disappeared, and a mixture of CuO and paratacamite, $\text{Cu}_2(\text{OH})_3\text{Cl}$, is formed. The Co cations remain either in solution or present in an amorphous phase. It was shown previously that thermal stability and crystallinity were highly dependent on the Cu/Al atomic ratio (Alejandre *et al.*, 1999).

IR spectra

The IR spectroscopy was performed on $(\text{Co}_{1-y}\text{Cu}_y)_2\text{Al}(\text{OH})_6\text{Cl}\cdot n\text{H}_2\text{O}$ ($0 \leq y \leq 1$) materials (Figure 4). The lattice vibrations appear in the 800 to 400 cm^{-1} frequency domain (Kloprogge and Frost, 1999). Two sharp absorbance peaks at 450 and 650 cm^{-1} are observed for $\{\text{Co}_2\text{Al}\}$. These contributions are assigned to $M-\text{O}$ lattice vibrations ($\text{Al}-\text{O}$ - and $\text{Co}-\text{O}$). With the substitution, the peaks of vibration become broader. The featureless spectrum is characteristic of highly disordered materials as reported for amorphous-like materials (Leroux *et al.*, 1999). The

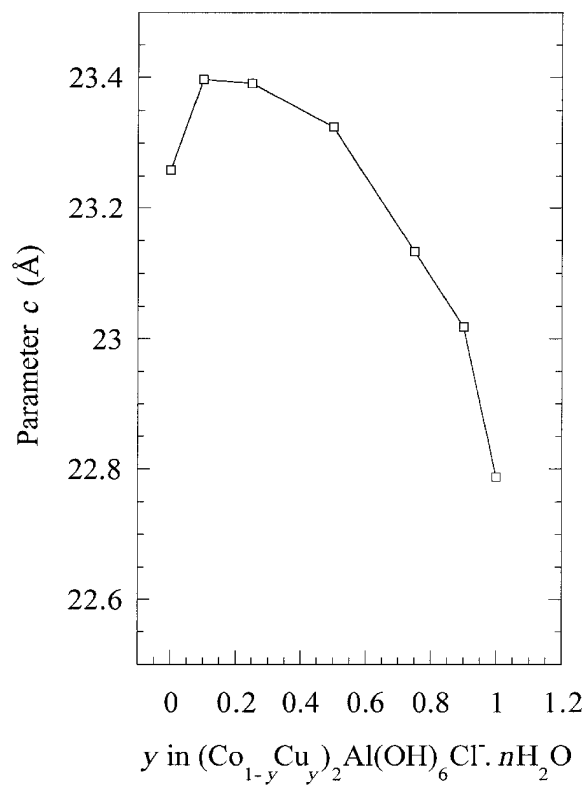


Figure 2. Variation of the c parameter.

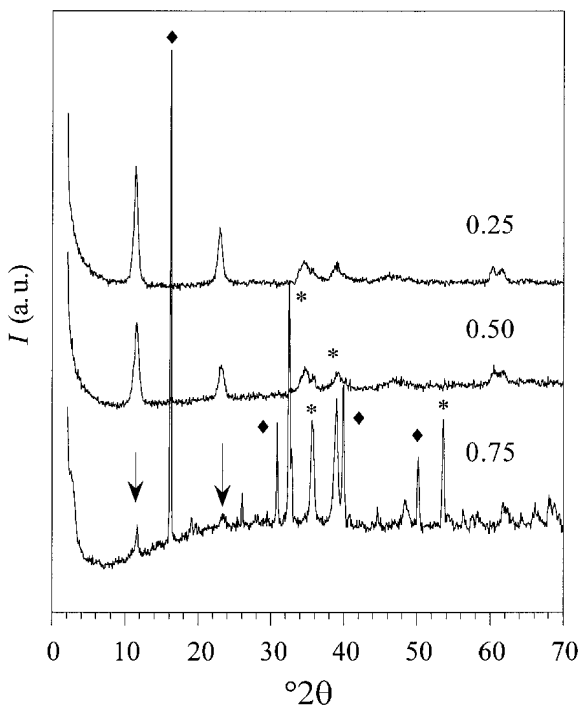


Figure 3. XRD patterns of selected samples after hydrothermal treatment. The y values in $\{(Co_{1-y}Cu_y)_2Al\text{-Cl}\}$ are reported. ◆ and * represent paratacamite, $Cu_2(OH)_3Cl$, and copper oxide, CuO , respectively.

OH-bending vibration occurs at $\sim 1620 \text{ cm}^{-1}$. Carbonate contamination is clearly observed; the stretching vibration, v_s , appears at $\sim 1370 \text{ cm}^{-1}$, its position characteristic of a symmetric coordination of the $-CO_3^{2-}$ (Prévost *et al.*, 2001); v_{as} is not clearly observed. The presence of carbonate anions has to be explained by the pH of the preparation and the basic surface of the synthetic materials, adsorbing carbonate anions from the atmosphere during the drying process. This contribution is largely reduced when the substitution is fully achieved ($y = 1$).

XAS study

Because of the lack of information concerning the intralamellar organization, XAS was performed to try to understand the local environment surrounding the transition metal atoms. The refinements of the reference samples agree well with the crystallographic data (Table 2). The moduli of the Fourier transforms are displayed in Figure 5. The first peak for both spectra at Cu and Co k -edge is ascribed to the shell of oxygen atoms. This contribution is constant with the substitution. The refinement gives a Cu–O distance of 1.97 \AA . An additional long Cu–O distance is introduced in the case of $y = 0.5$. Experimentally, two Cu–O shells were first considered in the refinement. A similar approach was undertaken for the local environment study of Cu cations into a substituted $\{\text{Mg}_2\text{Al}\}$ LDH-like phase

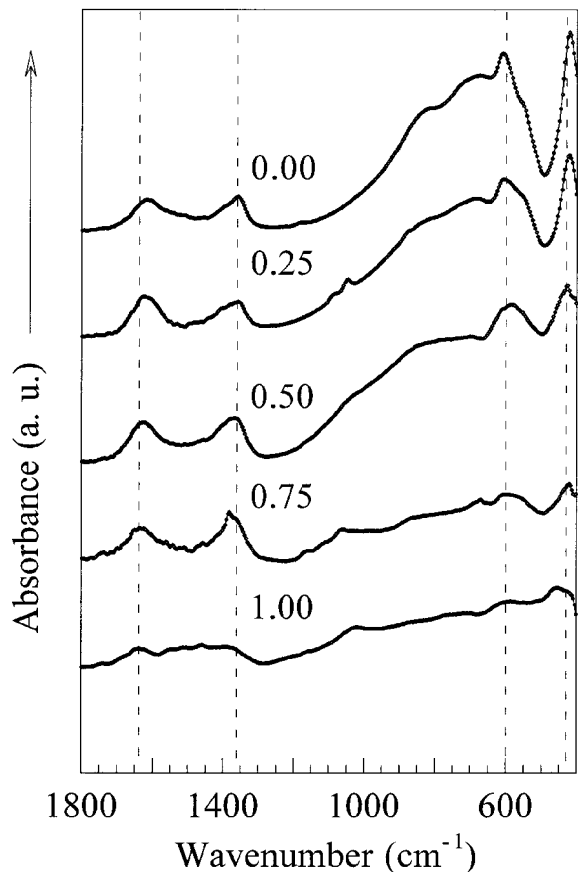


Figure 4. IR spectra of $(Co_{1-y}Cu_y)_2Al(OH)_6Cl.nH_2O$ ($0 \leq y \leq 1$). The values for y are reported.

(Köckerling *et al.*, 1997). The XAS fit results are reported in Tables 3 and 4 for Co and Cu k -edge studies, respectively. The quality of the fits is presented for the compositions $y = 0, 0.5$ and 1 in Figure 6. The Co–O distances are consistent with an octahedral coordination. It is noteworthy that Co–O is refined at a distance slightly greater than that for the Cu–O distance. Both transition cations are located in an octahedral oxygen environment, as underlined by the small pre-edge present on the XANES curves (Figure 7). The near-edge feature is highly sensitive to the first atomic cage surrounding the absorber. These data support the idea of LDH layers accommodating the substitution.

The metal-to-metal contribution is contained in the second peak of the Fourier transform. Due to their similar atomic numbers, Cu and Co atoms cannot be distinguished as distinct backscatters and are therefore grouped as *Me* in the refinements. Nevertheless it has been clearly shown that a study performed at different edges could shed some light on the organization as long as the energies of the edges are separated enough (Leroux *et al.*, 1999; Singh *et al.*, 2000). To get a better picture of the effect of the backscattering atoms on the EXAFS response, $\{\text{Cu}_2\text{Cr-Cl}\}$ (Roussel *et al.*, 2000) and

Table 2. XAS fit results and crystallographic data for reference samples, Co(OH)_2 , Cu(OH)_2 and CoAl_2O_4 .

Sample	Shell	<i>N</i>	<i>R</i> (Å)	σ^2 (10^{-3}\AA^2)	ρ (%) or JCPDF-data base
Co(OH)_2^*	O	6	2.097		
	Co	6	3.173		03-0913
	O	6	2.10	7.9	
	Co	6	3.17	8.1	2
Cu(OH)_2^{**}	O	2	1.929		
	O	2	1.943		
	O	2	2.633		
	Cu	4	2.949		35-505
	Cu	2	3.335		
	O	4	1.96	3.9	
	Cu	2	2.95	13	5
	Cu	4	3.34	13	
	$\text{Co(1)}^\ddagger > \text{O}$	4	1.938		
	$\rightarrow \text{Al(2)}$	18	3.361		
$\text{CoAl}_2\text{O}_4^\dagger$	$\rightarrow \text{Co(2)}$	18	3.361		
	$\rightarrow \text{Al(1)}$	4	3.510		
	$\rightarrow \text{Co(1)}$	4	3.510		
	$\text{Co(2)}^\ddagger > \text{O}$	6	1.927		(O'Neill, 1994)
	$\rightarrow \text{Al(2)}$	6	2.866		
	$\rightarrow \text{Co(2)}$	6	2.866		
	$\rightarrow \text{Co(1)}$	6	3.361		
	$\rightarrow \text{Al(1)}$	6	3.361		
	O\$	4.1	1.92	4.3	
	Al#	9.3	2.87	6.4	1.8
Co#	0.8	2.89	7.2		
	Co#	6.1	3.36	9.0	2.7

* Co(OH)_2 crystallizes in space group *P3m* with trigonal symmetry, lattice parameters of $a = 3.173 \text{ \AA}$ and $c = 4.640 \text{ \AA}$

** Cu(OH)_2 crystallizes in *Cmcm* space group with orthorhombic symmetry, lattice parameters of $a = 2.949 \text{ \AA}$, $b = 10.59 \text{ \AA}$ and $c = 5.256 \text{ \AA}$

\$ CoAl_2O_4 crystallizes in *Fd3m* space group with cubic symmetry, lattice parameter of $a = 8.107 \text{ \AA}$. Co(1) and Al(1) in 8a symmetry (*43m*), Co(2) and Al(2) in 16d (*3m*), O in 32e (*3m*)

\$ occupancy rate of [0.849] and [0.0755] for Co(1) and Co(2), respectively, and [0.151] and [0.9245] for Al(1) and Al(2), respectively, giving rise to $2\{0.849\text{Co(1)}+0.151\text{Al(1)}\}+4\{0.0755\text{Co(2)}+0.9245\text{Al(2)}\} = \text{Co}_2\text{Al}_4\text{O}_8$.

\$ Taking into account the rate occupancy and the difference of site for Co(1) and Co(2); the average oxygen coordination around Co is 4.25Co at 1.93 \AA .

Taking into account the rate occupancy and the difference of site for Co(1) and Co(2), the Co-Me environment is described as follows: 5.7 Al³⁺ at 2.866 \AA , 0.5 Co²⁺ at 2.866 \AA , 6.4 Co²⁺ at 3.361 \AA . The mean free path γ of 0.77 was found for the Co/Al backscattering contribution

{Cu₂Al-Cl} LDHs were compared at the Cu *k*-edge. A strong decrease of the second shell is observed between the {Cu₂Cr} and {Cu₂Al} samples as shown by the comparison of the modulus of the Fourier transforms (Figure 8). This is explained by the difference of backscattering amplitude between the trivalent cations (Cr³⁺, Al³⁺), and amplified with the destructive interference introduced by Al atoms. Indeed, the phase difference is ≈ 0 between Cu-Cr and Cu-Cu, and $\approx 3\pi/2$ between Cu-(Me) and Cu-Al for an absorber to backscatter distance of 3 \AA (McKale *et al.*, 1988). The refined distance between the Cu atoms and the cations (Co or Cu) ranges from 3.06 to 3.08 \AA , whereas the Co-Me distances are slightly larger. Conversely, the Co-Al distance is found to be shorter than that for

Cu-Al correlation. For the {Cu₂Al} composition, a second Cu-Cu shell needs to be introduced. To support this hypothesis, the $k\chi(k)$ signal was compared with the results obtained previously, in the absence of an additional Cu-Cu contribution (Figure 6e).

The peaks further away on the Fourier transform curves arise from multiple scattering effects (Alberding and Crozier, 1983), and are attributed to metallic neighbors. The second peak (at $2a$ distance from the central atom) is amplified by the so-called focusing effect due to three atoms lying linearly to each other (Roussel *et al.*, 2000). These contributions are present around Co atoms, whereas it is strongly reduced for the Cu environment and absent for the end-member {Cu₂Al}.

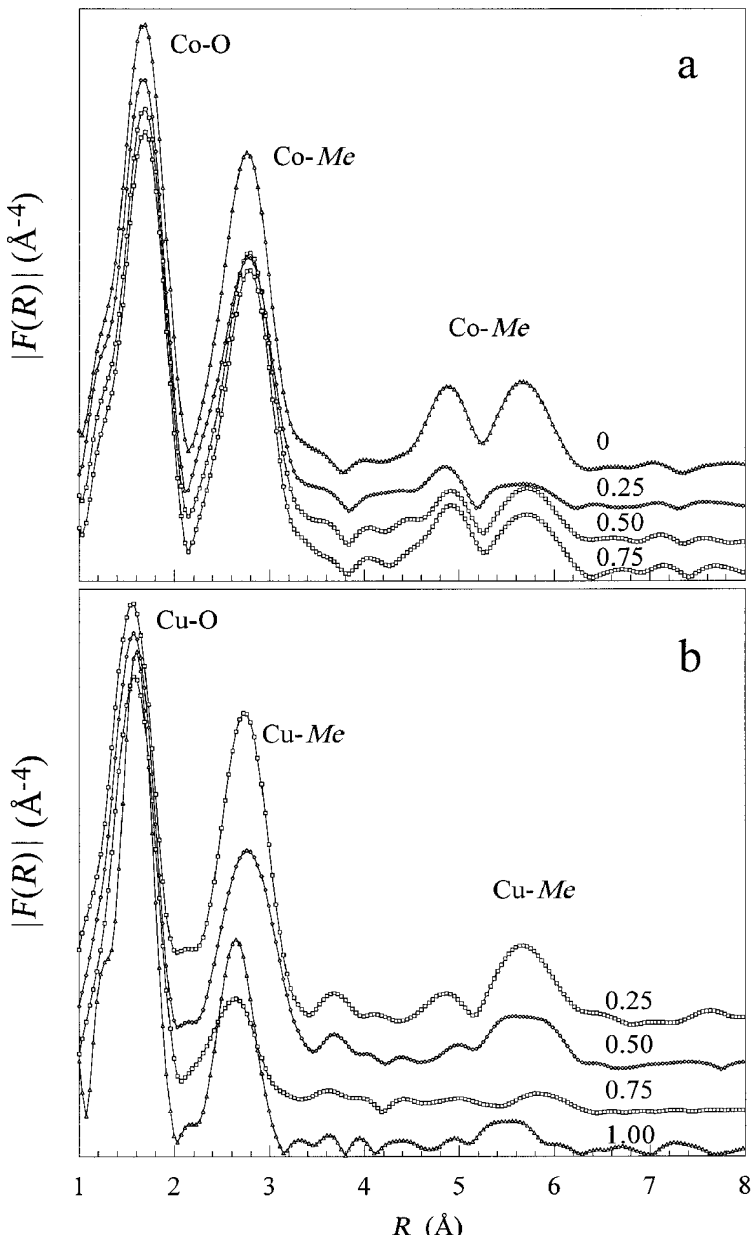


Figure 5. Moduli of the Fourier transform of $(Co_{1-y}Cu_y)_2Al(OH)_6Cl \cdot nH_2O$ ($0 \leq y \leq 1$) at (a) Co k -edge and (b) Cu k -edge. The values for y are reported. Distances are not corrected from the atomic potential phase shifts.

DISCUSSION

The ordered model predicts $3M^{II}$ and $3M^{III}$ around each divalent cation, and $6M^{II}$ around the trivalent cation (Hofmeister and Von Platen, 1992) for a ratio M^{II} to M^{III} of 2. Our results are consistent with the description. The refinements indicate a slight increase of Al atoms surrounding Cu^{2+} cations with the substitution. This may correspond to a cation segregation, but the variation is within the errors allowed by the technique. Because the Al atom content is constant in the materials (Table 1) and no depletion is observed around Co atoms, this hypothesis should be dismissed.

The XAS refinements clearly show that the cations (Cu, Co) polyhedra are not modified by the substitution of Cu in spite of the spreading of the $M-O$ band vibration observed by FTIR. Previous study has investigated the Cu atom environment in a 10% Cu-containing $\{Mg_2Al\}$ hydrotalcite-like phase (Köckerling *et al.*, 1997). Their finding was consistent with octahedra elongated by the Jahn-Teller effect. In our case, axial oxygen atoms are not depicted, a weak Cu–O contribution is found only for $y \leq 0.5$.

The environment for the transition cations is mainly unaffected by the substitution. A noticeable difference in

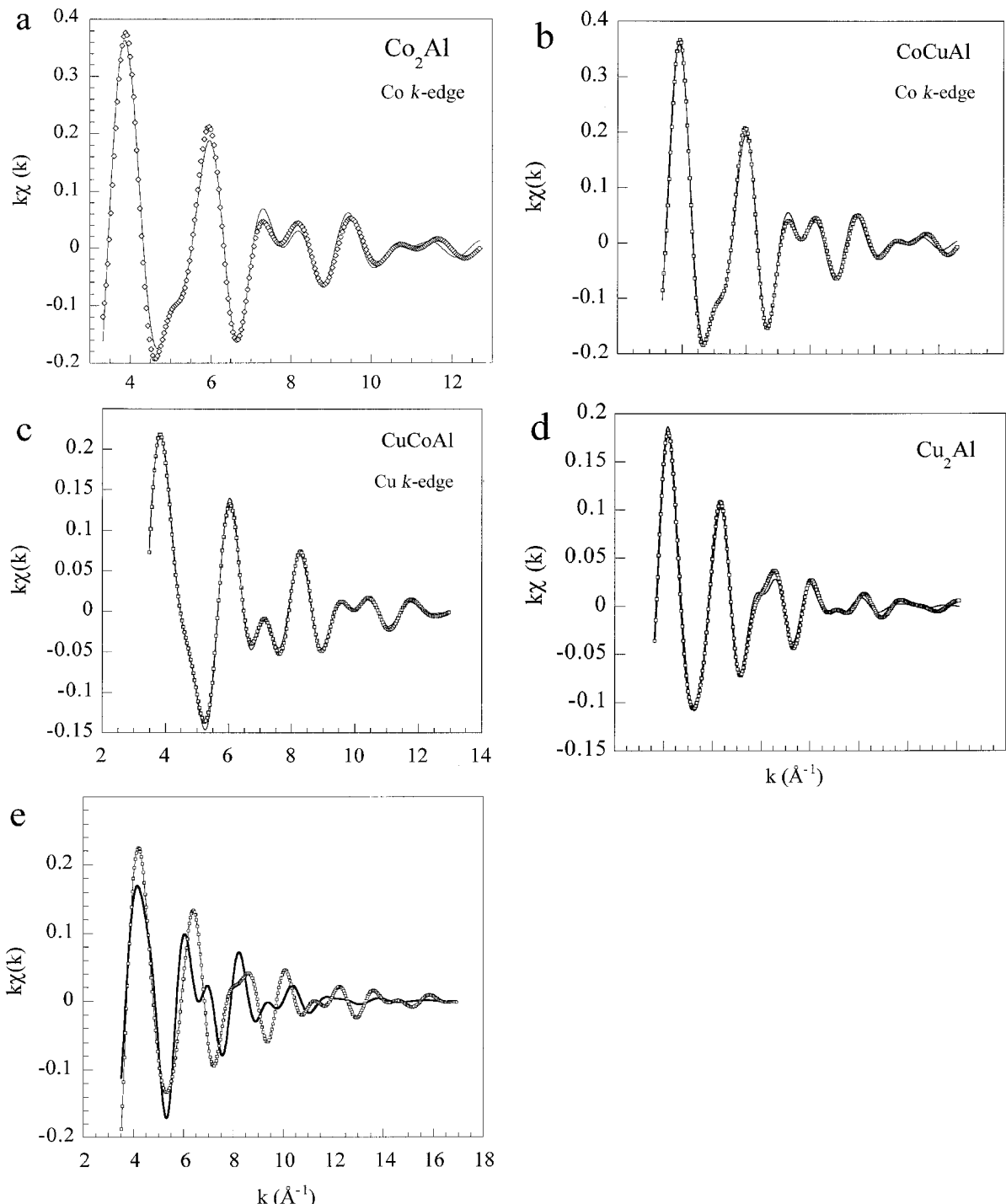


Figure 6. Refinement of the first two shells (-O, and -Me, Al) for $(\text{Co}_{1-y}\text{Cu}_y)_2\text{Al}(\text{OH})_6\text{Cl}\cdot n\text{H}_2\text{O}$, (a) $y = 0$, (b) $y = 0.5$ ($\text{Co } k\text{-edge}$), (c) $y = 0.5$ ($\text{Cu } k\text{-edge}$) and (d) $y = 1$. The refinement for $\{\text{Cu}_2\text{Al}\}$ using one Cu-Cu shell is displayed in (e) (see text). The dots represent the experimental data.

the metal to metal distance is observed, slightly exceeding the errors allowed by the XAS technique. This seems to indicate that the transition cations do not interact strongly with each other, *i.e.* do not mix at the

atomic scale, with the increase of y . This can be explained by: a phase mixture; the interstratification of the two cation aluminate sheets, as observed in the case of cationic mineral clays (Sakharov *et al.*, 1999), or

Table 3. Co *k*-edge EXAFS results for $(Co_{1-y}Cu_y)_2Al(OH)_6Cl.nH_2O$ ($0 \leq y \leq 1$).

Composition	Shell	<i>N</i>	<i>R</i>	σ^2 (10^{-3} Å 2)	ρ (%)
Co ₂ Al	Co-O	5.7	2.06	8.1	2
	Co-Al	2.6	3.09	10.	
	Co-Co	4.4	3.11	9.8	
Co _{1.5} Cu _{0.5} Al	Co-O	5.4	2.05	6.4	1
	Co-Me	5.0	3.12	9.4	
	Co-Al	4.9	3.11	9.8	
Co _{1.0} Cu _{1.0} Al	Co-O	5.8	2.06	8.1	5
	Co-Me	3.7	3.12	10.8	
	Co-Al	3.3	3.11	10.4	
Co _{0.5} Cu _{1.5} Al	Co-O	5.6	2.04	7.5	1
	Co-Me	3.5	3.12	10.8	
	Co-Al	3.3	3.11	10.4	

synthetic LDH materials (Thompson *et al.*, 1999); and the presence of (Co,Al) and (Cu,Al) clusters in the sheets, as shown for Ni clay minerals (Manceau and Calas, 1986).

As indicated by XRD (Figure 1), a solid-solution is present in the range $0 \leq y \leq 0.75$. No great broadening of the diffraction peaks is observed as for interstratified material (Rajamathi *et al.*, 2000). Therefore, the monotonous decrease of the second coordination shell cannot be explained either by the presence of phase mixture or

Table 4. Cu *k*-edge XAS results for $(Co_{1-y}Cu_y)_2Al(OH)_6Cl.nH_2O$ ($0 \leq y \leq 1$).

Composition	Shell	<i>N</i>	<i>R</i>	σ^2 (10^{-3} Å 2)	ρ (%)
Cu ₂ Al	Cu-O	5.3	1.97	5.8	1.1**
	Cu-Cu	2.3	3.00	12.3	
	Cu-Cu	1.6	3.17	17.2	
Cu _{1.5} Co _{0.5} Al	Cu-Al*	3.6	3.14	15.0	0.5
	Cu-O	4.0	1.96	5.8	
	Cu-Me	1.4	3.06	8.1	
Cu _{1.0} Co _{1.0} Al	Cu-Al	3.0	3.19	12.5	0.5
	Cu-O	4.2	1.97	6.7	
	Cu-O	0.3	2.18	6.7	
Cu _{0.5} Co _{1.5} Al	Cu-Me	2.2	3.07	12.0	0.5
	Cu-Al	2.2	3.19	14.0	
	Cu-O	4.5	1.98	7.0	
Cu _{0.5} Co _{1.5} Al	Cu-O	0.6	2.26	7.0	0.5
	Cu-Me	2.6	3.08	10.0	
	Cu-Al	1.8	3.17	14.4	

* mean free path $\gamma_{Cu/Al}$ was taken equal to $\gamma_{Co/Al}$ from the $CoAl_2O_4$ refinement (Table 2)

** fit is of 25% in absence of the Al shell

by any phenomenon of interstratification. Moreover it would be rather unrealistic, from a stability point of view, for {Co₂Al} regular sheets to face {Cu₂Al}. Presumably, the increase in the Debye-Waller factor

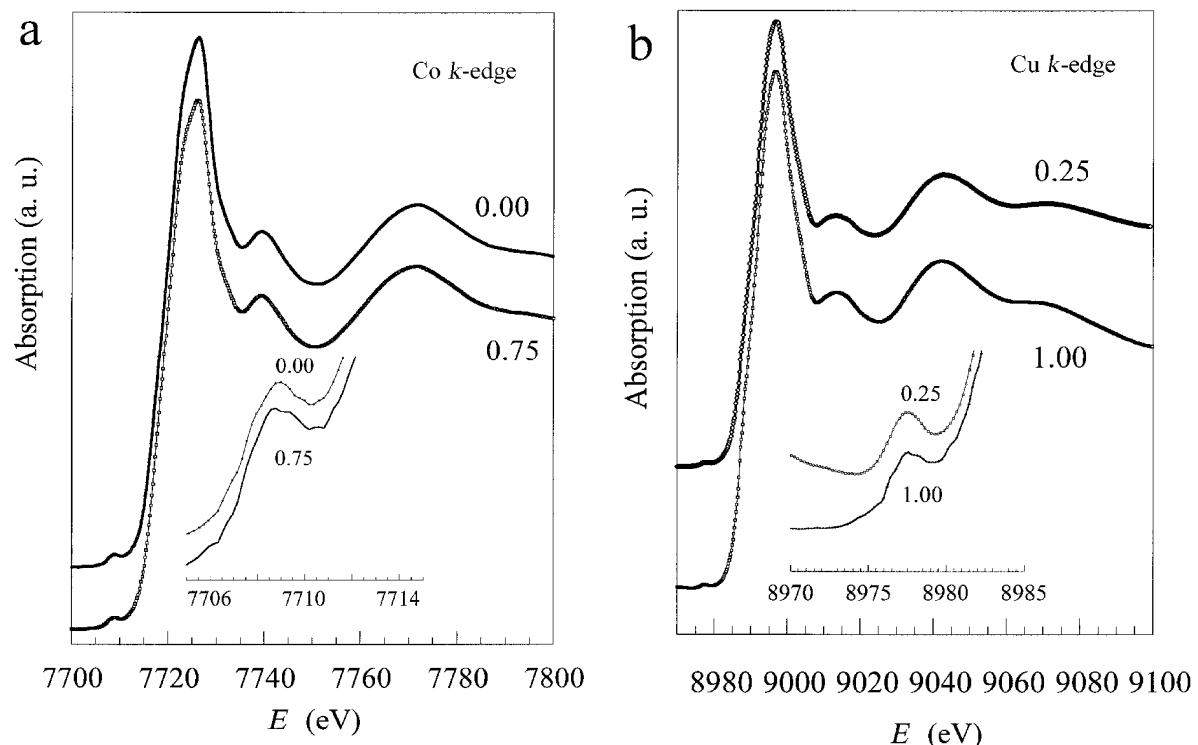


Figure 7. XANES spectra of $(Co_{1-y}Cu_y)_2Al(OH)_6Cl.nH_2O$ ($0 \leq y \leq 1$) at (a) Co *k*-edge and (b) Cu *k*-edge. The values for y are reported. The spectra are offset for clarity.

shows that a local disorder is present around the Cu cations for the $\{\text{Cu}_2\text{Al}\}$ composition.

A more reasonable explanation is the presence of two types of domain $\{\text{Co}_2\text{Al}\}$ and $\{\text{Cu}_2\text{Al}\}$. The same approach has been undertaken to understand the formation of NiPS_3 amorphous material by the ‘chimie douce’ route (Fragnaud *et al.*, 1993) or the intracrystalline distribution in some clay minerals (Manceau and Calas, 1986). By varying the $\{\text{Co}_2\text{Al}\}$ domain size, the contribution of the bulk material is distinguished from its border. Figure 9 gives the relative part of each absorber to backscatter (Co–Co and Co–Cu) contributing to the second shell, this depending on the $\{\text{Co}_2\text{Al}\}$ domain size. It is clearly shown that a size ranging between 5 and 10 nm² would give rise to an important excess of Co atoms, the border effect representing <10% of all the transition cation neighbors. As observed by microscopy, the platelets are in the order of 100 to 300 nm in size, allowing hypothetically a large number of domains (>3000). This may explain the absence of phase separation for $y = 0.5$. The size of (Cu,Al) domains can be estimated from the average number of second neighbors. This results in a mean area diameter of 25 to 50 Å, close to the values observed for Ni clay minerals (Manceau and Calas, 1986).

The $\{\text{Co}_2\text{Al}\}$ ‘cluster’ has a brucitic intralayer arrangement in agreement with the structural refinement of $\text{Co}_2\text{Al}(\text{OH})_6\text{Cl}$. The refined XAS distances for

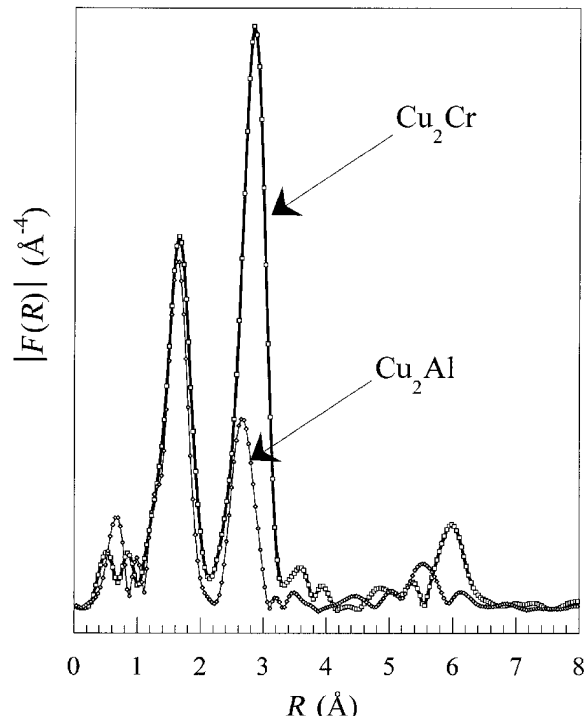


Figure 8. Comparison of the moduli of the Fourier transform for $\{\text{Cu}_2\text{Cr}\}$ (Roussel *et al.*, 2000) and $\{\text{Cu}_2\text{Al}\}$ LDH-like phases at Cu k -edge. Distances are not corrected for phase shift.

$\{\text{Cu}_2\text{Al}\}$ are close to the data reported for the local structure of the two-dimensional $\text{Cu}_2(\text{OH})_3X$ copper hydroxide (X is an interlayer anion, paratacamite is obtained when $X = \text{Cl}$) (Jiménez-Lopez *et al.*, 1993; Fujita *et al.*, 1997). This material exhibits a botallackite-type structure in which Cu atoms have two distinct sites of coordination [4+2] and [4+1+1], and the distorted CuO_6 polyhedra are sharing edges. Three Cu–Cu distances (3.02, 3.15 and 3.25 Å) are found for the botallackite (Jiménez-Lopez *et al.*, 1993). In our sample, the amplitude of the second peak is not constant, indicating the presence of a second type of neighbor, Al^{3+} cations. This leads us to suggest that Al atoms are closely related to Cu atoms, dismissing any formation of copper hydroxide phases such as $\text{Cu}(\text{OH})_2$, $\text{Cu}_2(\text{OH})_3X$ or what was reported for Co hydrotalcite-like phases in which the positive charge of the layers was restored by a partial protonation of the hydroxyl ions compensating the absence of trivalent ions (Kamath *et al.*, 1997). The local order of Cu atoms in $\{\text{Cu}_2\text{Al}\}$ is described from $\text{Cu}_2(\text{OH})_3X$ with some of the Cu^{2+} cations replaced by Al^{3+} .

This may be extended to the substituted materials. For low y values, the second shell is not modified, and the linear cation arrangement is present. The CuO_6 polyhedra are then intimately mixed with the LDH-like framework. With the increase of y , Cu polyhedra segregate into domains, and finally, its local structure changes from brucite to a botallackite-type structure. The loss of linear arrangement around the Cu atoms is evidenced by the disappearance of the focusing effect (FE) peaks (Figure 5). This may be explained by highly corrugated $\{\text{Cu}_2\text{Al}\}$ domains surrounded by ordered $\{\text{Co}_2\text{Al}\}$ domains. It is noteworthy that the FE peaks are

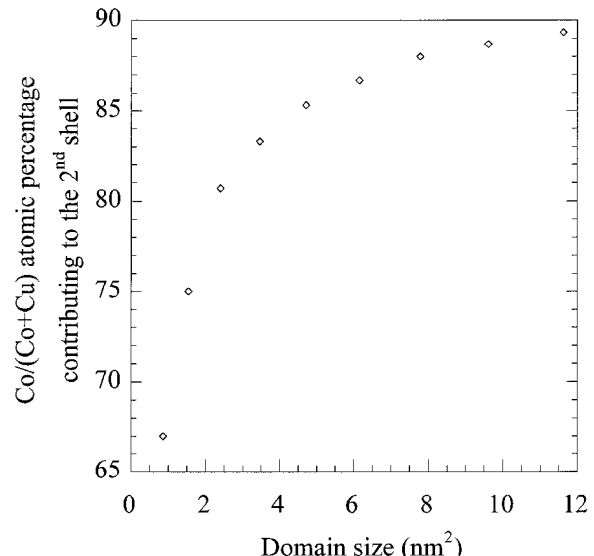


Figure 9. Variation of the number of neighbors of the second shell as a function of $\{\text{Co}_2\text{Al}\}$ domain size.

observed for the basic Cu salt (Jiménez-Lopez *et al.*, 1993). This shows that Al³⁺ cations induce a strong distortion of the layers, thus preventing the formation of paratacamite or botallackite-type structures on a large scale. Additionally, the local LDH-like structure is restored by a small number of CoO₆ polyhedra ($y = 0.25$).

CONCLUSIONS

It was established that Cu²⁺ cations have a destabilizing effect as shown by the structural comparison of {Cu₂Cr} and {Zn₂Cr} LDH-like phases (Roussel *et al.*, 2000). These phases are described in the $R\bar{3}m$ and $P\bar{3}1$ space groups, respectively. With the substitution in (Co_{1-y}Cu_y)₂Al(OH)₆Cl_nH₂O ($0 \leq y \leq 1$), it was shown, in the present work, that Cu and Co cations do not present the same local environment. In particular, this was shown by the second coordination shell and with the correlation arising from linear cation arrangement. Finally, it was found that the local structure surrounding Cu cations changes from a brucite to botallackite-type environment with the substitution. The description of the Cu-substituted phases as intralayer domains explains reasonably well the results gathered by the XRD and XAS techniques.

ACKNOWLEDGMENTS

The authors are very grateful to Dr S. Guggenheim and to an anonymous referee for their critical reviews and helpful suggestions.

REFERENCES

- Aitchison, P., Ammundsen, B., Jones, D.J., Burns, G. and Rozière, J. (1999) Cobalt substitution in lithium manganate spinels: examination of local structure and lithium extraction by XAFS. *Journal of Material Chemistry*, **9**, 3125–3130.
- Alberding, N. and Crozier, E.D. (1983) Multiple scattering and disorder in extended X-ray absorption fine structure analysis. *Physical Reviews B*, **27**, 3374–3382.
- Alejandre, A., Medina, H., Salagre, P., Correig, X. and Sueiras, J.E. (1999) Preparation and study of Cu-Al mixed oxides via hydrotalcite-like precursors. *Chemistry of Materials*, **11**, 939–948.
- Bellotto, M., Rebours, B., Clause, O., Lynch, J., Bazin, D. and Elkaïm, E. (1996) A reexamination of hydrotalcite crystal chemistry. *Journal of Physical Chemistry*, **100**, 8527–8534.
- Bessonenev, A.V., Fogg, A.M., Francis, R.J., Price, S.J. and O'Hare, D. (1997) Synthesis and structure of gibbsite intercalation compounds [LiAl₂(OH)₆]X {X=Cl, Br, NO₃} and [LiAl₂(OH)₆]Cl. H₂O using synchrotron X-ray and neutron powder diffraction. *Chemistry of Materials*, **9**, 241–247.
- Bookin, A.S., Cherkashin, V.I. and Drits, V.A. (1993) Polytype diversity of the hydrotalcite-like minerals. II Determination of the polytypes of experimentally studied varieties. *Clays and Clay Minerals*, **41**, 558–564.
- Carrao, K.A. and Wasserman, S.R. (1996) Stability of Cu(II) and Fe(III) porphyrins on montmorillonite clay: an X-ray absorption study. *Chemistry of Materials*, **8**, 219–225.
- Fragaud, P., Prouzet, E., Ouvrard, G., Mansot, J.-L., Payen, C., Brec, R. and Dexpert, H. (1993) Room temperature synthesis study of highly disordered a-Ni₂P₂S₆. *Journal of Non-crystalline Solids*, **160**, 1–17.
- Fujita, W., Awaga, K. and Yokoyama, T. (1997) EXAFS study of two dimensional hybrid nanocomposites, Cu₂(OH)₃(n-C_mH_{2m+1}COO) (m=0,1,7,8,9): structural modification in the inorganic layer induced by the interlayer organic molecule. *Inorganic Chemistry*, **36**, 196–199.
- Hofmeister, W. and Von Platen, H. (1992) Crystal chemistry and atomic order in brucite-related double-layer structures. *Crystal Review*, **3**, 3–29.
- Jiménez-Lopez, A., Rodriguez-Castellon, R., Olivera-Pastor, P., Maireles-Torres, P., Tomlinson, A.A.G., Jones, D.J. and Rozière, J. (1993) Layered basic copper anion exchangers: chemical characterisation and X-ray absorption study. *Journal of Materials Chemistry*, **3**, 303–307.
- Kamath, P.V., Therese, G.H. and Gopalakrishnan, J. (1997) On the existence of hydrotalcite-like phases in the absence of trivalent cations. *Journal of Solid State Chemistry*, **128**, 38–41.
- Kloprogge, J.T. and Frost, R.L. (1999) Fourier transform infrared and Raman spectroscopic study of the local structure of Mg-, Ni-, and Co-hydrotalcites. *Journal of Solid State Chemistry*, **146**, 506–515.
- Köckerling, M., Geismar, G., Henkel, G. and Nolting, H.-F. (1997) X-ray absorption spectroscopic studies on copper-containing hydrotalcite. *Journal of the Chemical Society, Faraday Transactions*, **93**, 481–484.
- Leroux, F., Piffard, Y., Ouvrard, G., Mansot, J.-L. and Guyomard D. (1999) New amorphous mixed transition metal oxides and their Li derivatives: synthesis, characterization, and electrochemical behavior. *Chemistry of Materials*, **11**, 2948–2959.
- Leroux, F., Adachi-Pagano, M., Intissar, M., Chauvière, S., Forano, C. and Besse, J.-P. (2001a) Delamination and restacking of layered double hydroxides. *Journal of Materials Chemistry*, **11**, 105–112.
- Leroux, F., Moujahid, El M., Taviot-Guého, C. and Besse, J.-P. (2001b) Effect of layer charge modification for Co-Al layered double hydroxides: study by X-ray absorption spectroscopy. *Solid State Sciences*, **3**, 81–92.
- Malherbe, F., Bigey, L., Forano, C., de Roy, A. and Besse, J.-P. (1999) Structural aspects and thermal properties of takovite-like layered double hydroxides pillared with chromium oxo-anions. *Journal of the Chemical Society, Dalton Transactions*, 3831–3839.
- Manceau, A. and Calas, G. (1986) Nickel-bearing clay minerals: II Intracrystalline distribution of nickel: an X-ray absorption study. *Clay Minerals*, **21**, 341–360.
- McKale, A.G., Veal, B.W., Paulikas, A.P., Chan, S.-K. and Knapp, G.S. (1988) Improved ab initio calculations of amplitude and phase functions for extended X-ray absorption fine structure spectroscopy. *Journal of the American Chemical Society*, **110**, 3763–3768.
- Miyata, S. (1983) Anion-exchange properties of hydrotalcite-like compounds. *Clays and Clay Minerals*, **31**, 305–311.
- O'Neill, H.St.C. (1994) Temperature dependence of the cation distribution in CoAl₂O₄ spinel. *European Journal of Mineralogy*, **6**, 603–609.
- Prévot, V., Forano, C. and Besse, J.-P. (2001) Hybrid derivatives of layered double hydroxides. *Applied Clay Science*, **18**, 3–15.
- Rajamathi, M., Kamath, V. and Seshadri, R. (2000) Polymorphism in nickel hydroxide: role of interstratification. *Journal of Material Chemistry*, **10**, 503–506.
- Roussel, H., Briois, V., Elkaïm, E., de Roy, A. and Besse, J.-P. (2000) Cationic order and structure of [Zn-Cr-Cl] and [Cu-Cr-Cl] layered double hydroxides: an XRD and EXAFS study. *Journal of Physical Chemistry B*, **104**, 5915–5923.
- Sakharov, B.A., Lindgreen, H., Salyn, A.L. and Drits V.A.

- (1999) Mixed-layer kaolinite-illite-vermiculite in North Sea shales. *Clay Minerals*, **34**, 333–344.
- Shimizu, K., Maeshima, H., Yoshida, H., Satsuma, A. and Hattori, T (2000) Spectroscopic characterisation of Cu-Al₂O₃ catalysts for selective reduction of NO with propene. *Physical Chemistry Chemical Physics*, **2**, 2435–2439.
- Singh, B., Sherma, D.M., Gilkes, R.J., Wells, M. and Mosselmans, J.F.W. (2000) Structural chemistry of Fe, Mn and Ni in synthetic hematites as determined by extended X-ray absorption fine structure spectroscopy. *Clays and Clay Minerals*, **48**, 521–528.
- Thiel, J.-P., Chiang, C.K. and Poeppelmeier, K.R. (1993) Structure of LiAl₂(OH)₇·2H₂O. *Chemistry of Materials*, **5**, 297–304.
- Thompson, H.A., Parks, G.A. and Brown, G.E., Jr. (1999) Ambient-temperature synthesis, evolution, and characterization of cobalt-aluminum hydrotalcite-like solids. *Clays and Clay Minerals*, **47**, 425–438.
- Trombetta, M., Ramis, G., Busca, G., Montanari, B. and Vaccari, A. (1997) Ammonia adsorption and oxidation on Cu/Mg/Al mixed oxide catalysts prepared via hydroxide-type precursors. *Langmuir*, **13**, 4628–4637.
- Vucelic, M., Jones, W. and Moggridge, G.D. (1997) Cation ordering in synthetic layered double hydroxides. *Clays and Clay Minerals*, **45**, 803–813.
- Velu, S., Sabde, D.P., Shah, N. and Sivasanker, S. (1998) New hydroxyl-like anionic clays containing Zr⁴⁺ in the layers: synthesis and physicochemical properties. *Chemistry of Materials*, **10**, 3451–3458.

(Received 26 July 2000; revised 14 July 2001; Ms. 474; A.E. James E. Amonette)